Supplemental Material

Supplemental Material for "Decomposing the Drivers of Polar Amplification with a Single Column Model"

Matthew Henry*

College of Engineering, Mathematics and Physical Sciences, University of Exeter, Exeter, UK

Timothy M. Merlis

Department of Atmospheric and Oceanic Sciences, McGill University, Montreal, Quebec, Canada

Nicholas J. Lutsko

Scripps Institution of Oceanography, University of California at San Diego, La Jolla, CA, USA

Brian E.J. Rose

Department of Atmospheric and Environmental Sciences, University at Albany (State University of New York), USA

**Corresponding author address:* Matthew Henry, College of Engineering, Mathematics and Physical Sciences, Harrison Building, Streatham Campus, University of Exeter, North Park Road, Exeter, UK, EX4 4QF.

E-mail: m.henry@exeter.ac.uk

ABSTRACT

LIST OF TABLES

Experiment	Tropics	Pole (4xCO_2)	Pole (4xCO_2+12)	Pole (4xCO_2+24)
CO_2	30.0	26.2	26.2	26.2
q (local and remote)	30.0	26.2	26.2	26.2
Diffusion	30.0	26.2	26.2	26.2
ET (dry and moist)	30.0	26.2	26.2	26.2
Q_s	N/A	N/A	34.5	40.5
All	30.0	26.2	34.5	40.5

Table S1. Value of the bias term (Q_{bias} in $\mathrm{W\,m^{-2}}$) for each single column model experiment. Q_{bias} accounts for the difference between the GCM's surface turbulent (sensible and latent) heat fluxes and the SCM's surface convection term, and the bias in net surface shortwave radiation. When a surface heat source (Q_S) is present at high latitudes, the surface turbulent heat fluxes are smaller, hence Q_{bias} is reduced.

LIST OF FIGURES

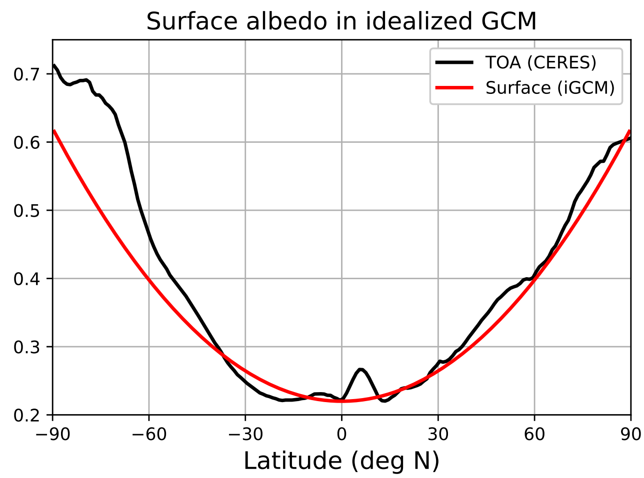

Fig. S1. Surface albedo used in idealized GCM calculated using following formula: $0.22 + 0.4 * (lat/90)^2$ (red). Annual-mean zonally averaged climatology (07/2005 - 06/2015) of top-of-atmosphere albedo with data from Cloud and the Earth's Radiant Energy System (CERES) (black).

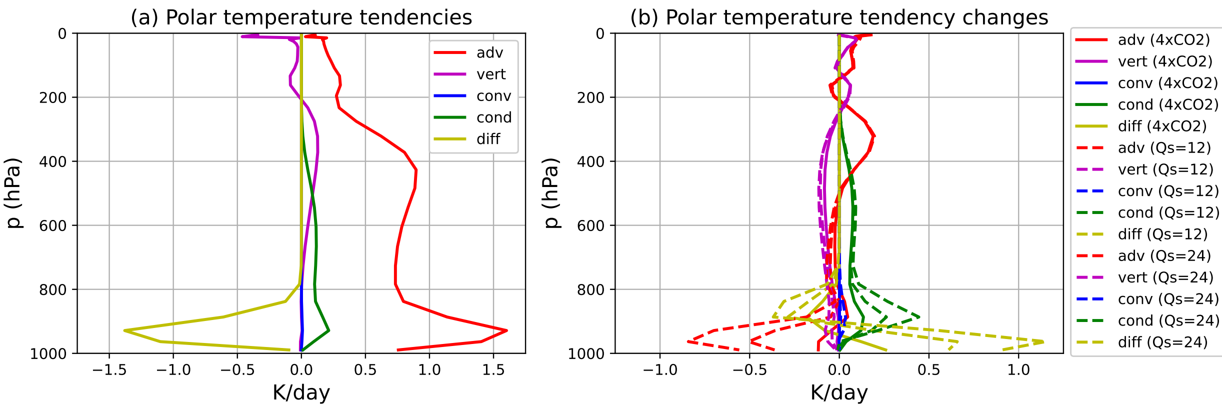

Fig. S2. (a) Climatological and (b) changes in idealized GCM temperature tendencies averaged poleward of 80° North. Shown are the dry (‘adv’ in red) and moist (‘cond’ in green) components of the energy transport, the vertical component of the advection term (‘vert’ in magenta), and the convective (‘conv’ in blue) temperature tendency. The first two are used as input to the single column model.

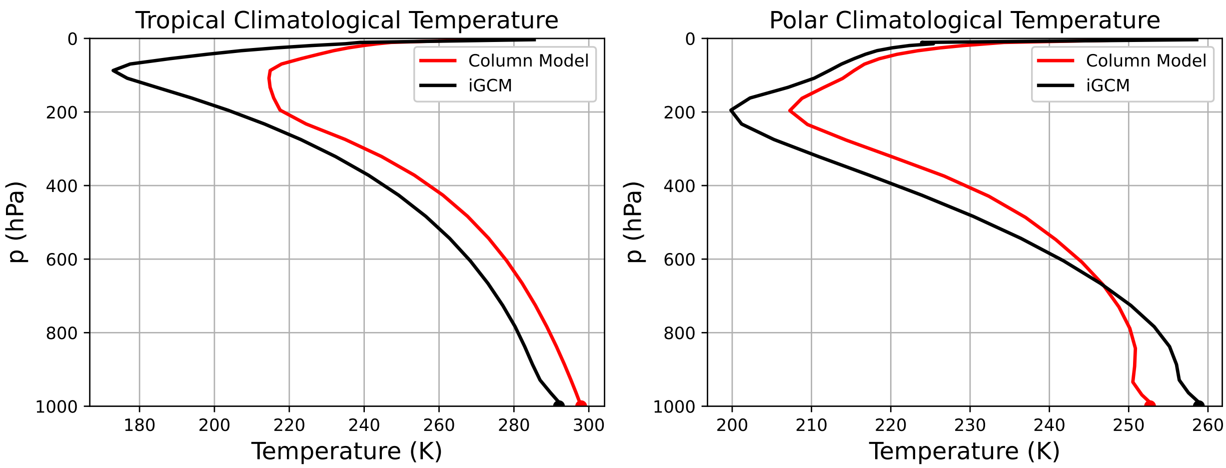

Fig. S3. Analog of figure 2 in the main text but with tropical and polar latitudinal bound set at 20° and 60° respectively. Climatological temperature of the idealized GCM (black) and the single column model (red).

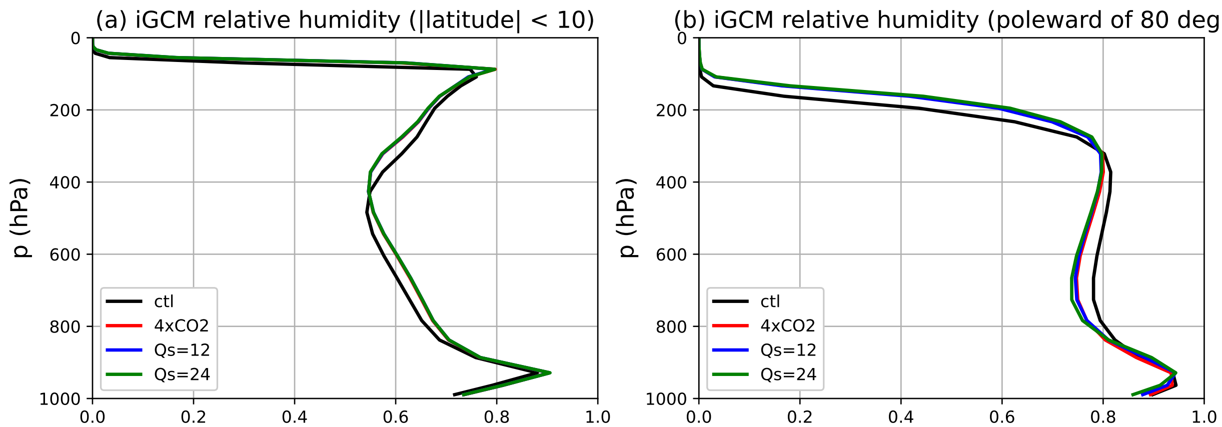

Fig. S4. Relative humidity of the idealized GCM averaged from -10° to 10° North (a) and poleward of 80° North (b) for the control (black), $4xCO_2$ (red), $4xCO_2$ with a 12 $W\,m^{-2}$ surface heat source (blue), and $4xCO_2$ with a 24 $W\,m^{-2}$ surface heat source (green) simulations.

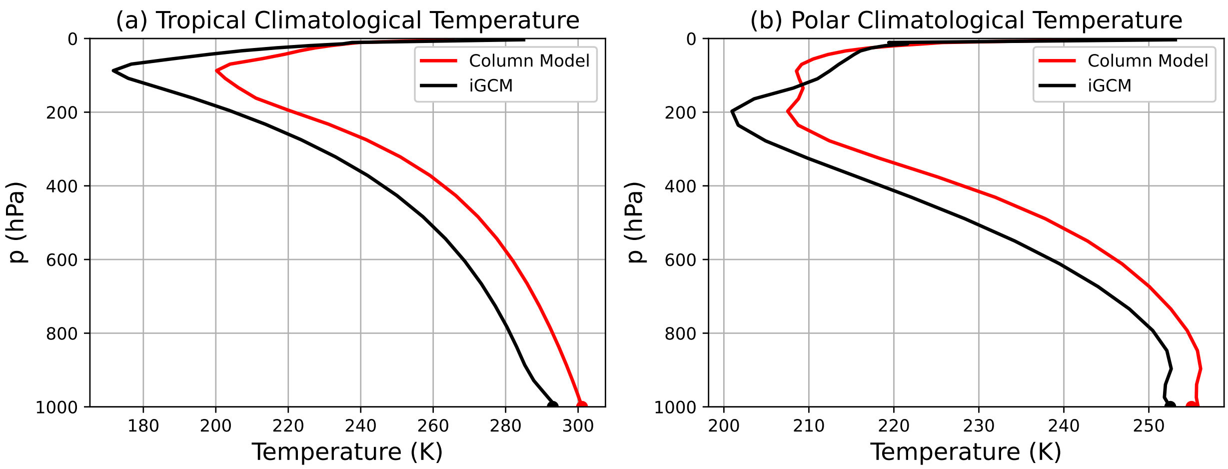

Fig. S5. Comparison of the climatological temperature of the fixed relative humidity single column model (red) and the idealized atmospheric GCM (black) in the tropics (a) and the pole (b) for the 4xCO_2 experiment only.

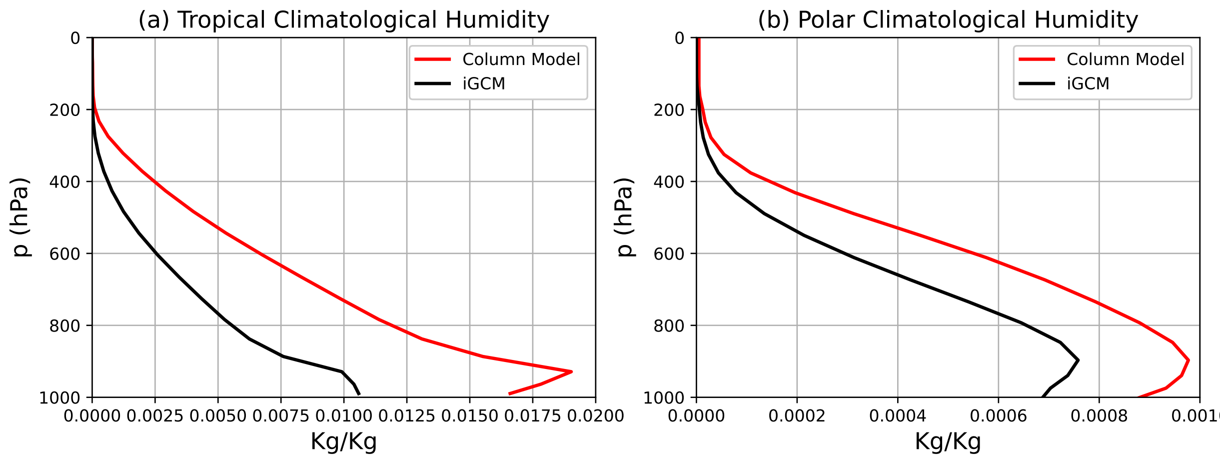

Fig. S6. Comparison of the climatological specific humidity of the fixed relative humidity single column model (red) and the idealized atmospheric GCM (black) in the tropics (a) and the pole (b) for the 4xCO_2 experiment only.

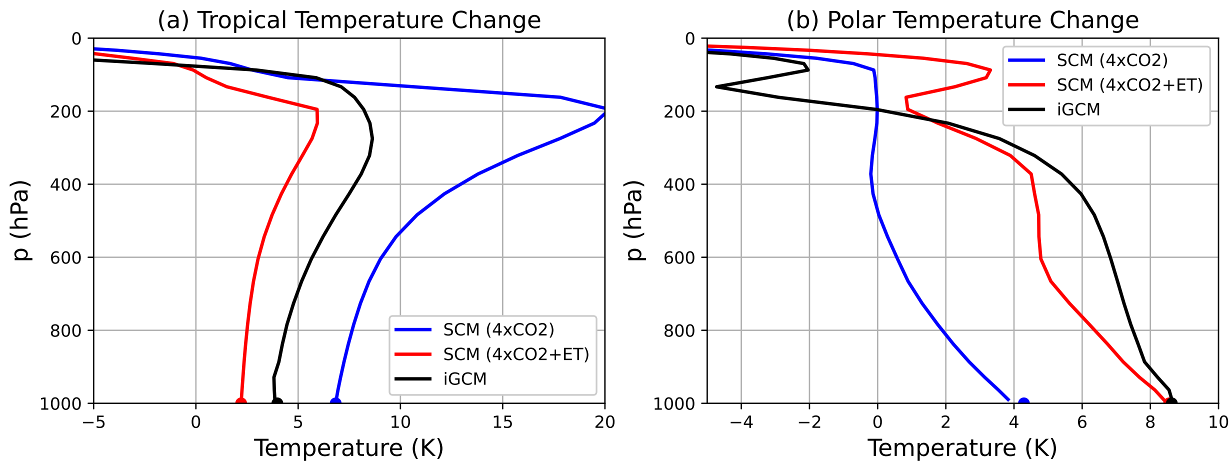

Fig. S7. Comparison of temperature change between the fixed relative humidity single column model (with control atmospheric energy transport (blue) and perturbed atmospheric energy transport (red)) and the idealized atmospheric GCM (black) in the tropics (a) and high latitudes (b) for the 4xCO_2 experiment only.

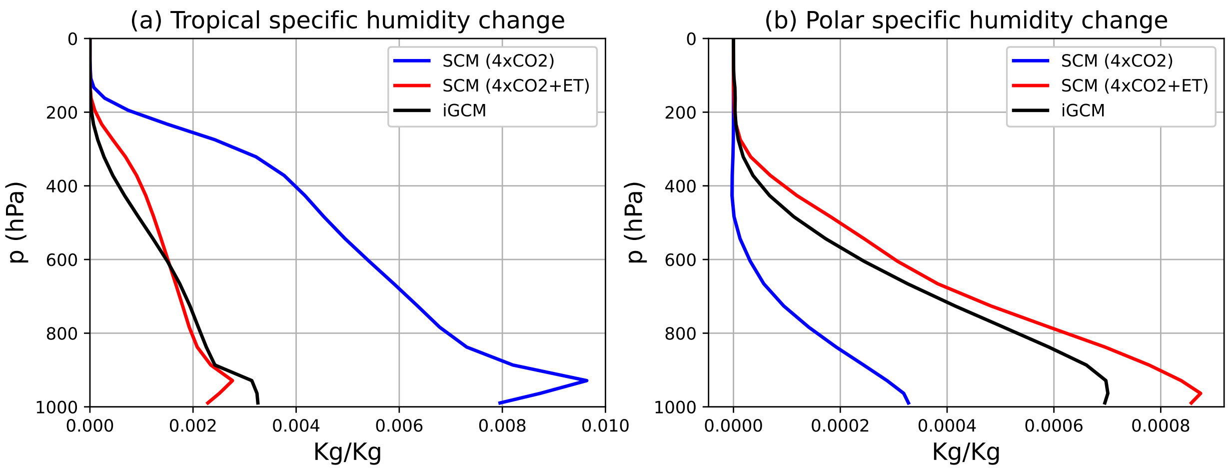

Fig. S8. Comparison of specific humidity change between the fixed relative humidity single column model (with control atmospheric energy transport (blue) and perturbed atmospheric energy transport (red)) and the idealized atmospheric GCM (black) in the tropics (a) and high latitudes (b) for the 4xCO_2 experiment only.